Smart Soccer Shoe: Monitoring Foot-Ball Interaction with Shoe Integrated Textile Pressure Sensor Matrix

Bo Zhou
German Research Center for A.I. (DFKI GmbH)
Kaiserslautern, Germany
bo.zhou@dfki.de

Markus Wirth
Friedrich-Alexander University (FAU)
Erlangen, Germany
markus.wirth@fau.de

Christine Martindale
Friedrich-Alexander University (FAU)
Erlangen, Germany
christine.f.martindale@fau.de

Harald Koerger
adidas AG
Herzogenaurach, Germany
Harald.Koerger@adidas.com

Constantin Zwick
adidas AG
Herzogenaurach, Germany
Constantin.Zwick@adidas.com

Heber Cruz
DFKI GmbH
Kaiserslautern, Germany
heber.cruz@dfki.de

Bjoern Eskofier
Friedrich-Alexander University (FAU)
Erlangen, Germany
bjoern.eskofier@fau.de

Paul Lukowicz
DFKI GmbH & TU Kaiserslautern
Kaiserslautern, Germany
paul.lukowicz@dfki.de

ABSTRACT

In this paper we present a smart soccer shoe that uses textile pressure sensing matrices to detect and analyze the interaction between players' foot and the ball. We describe the sensor system that consists of two 3×4 and one 3×3 matrices sampled at over 500Hz with low power electronics that allows continuous operation (incl. wireless transmission) for 8 hours using a small 800mA/h Li-Po battery. We show how relevant parameters for shot analysis such as contact speed and contact angles can be reliably derived from the sensor signals. To ensure reliable ground truth we evaluated the system with a kick robot in the adidas testing facility, which is the standard approach used by adidas to systematically and quantitatively test new shoes and balls. The test encompasses 17 different types of shots and achieves a near 100% classification accuracy/F-score. The system endured extreme levels of impact resulting in over $100 km/hr$ ball speed.

Author Keywords

wearable system; smart textiles; pressure mapping; digital sport; soccer shoe; activity recognition

ACM Classification Keywords

J.m. Computer Applications: Miscellaneous

ISWC '16, September 12-16, 2016, Heidelberg, Germany
 ISBN 978-1-4503-4460-9/16/09...$15.00
DOI: http://dx.doi.org/10.1145/2971763.2971784

INTRODUCTION

As the world's most popular sport [16], much research effort has been put into the study of the science behind soccer [18]. From the classic projectile mathematics models [4][9] to the more recent aerodynamics of the ball's flight path [14][15] [3][11]that concerns the influence of a wider range of factors such as spin, surface roughness and the seam geometry of patches. Those studies cover trajectory data measured by high-speed camera systems both from real players and launching machines. Wearable systems to study kinematics and detect shot/pass actions based on inertial measurement units (IMU) are also being investigated [2][20]. However, the actual physical contact of launching a ball (between the shoe surface and the ball) has not been sufficiently studied. The lack is mainly due to the constraints that the instrumentation should not change the physical properties of the contact surface, which is soft and irregular in shape; and that the impact time can be less than 20 milliseconds, making it difficult for tether-free implementations.

Contribution

We have developed a solution that overcomes the above problems allowing detailed monitoring of the interaction between the shoe and the ball. The solution is based on our textile pressure sensor matix technology [6] that we have previously applied to the monitoring of gym exercises [21] [24]. Addressing the specific case of a smart soccer shoe, this paper makes the following contributions:

- We developed a specific sensing setup for the soccer shoe. We covered the mostly engaged surface area on the shoe (Figure 1) with fabric pressure sensors. The electronics includes high speed Bluetooth Classic wireless data transmission and miniaturized footprint.

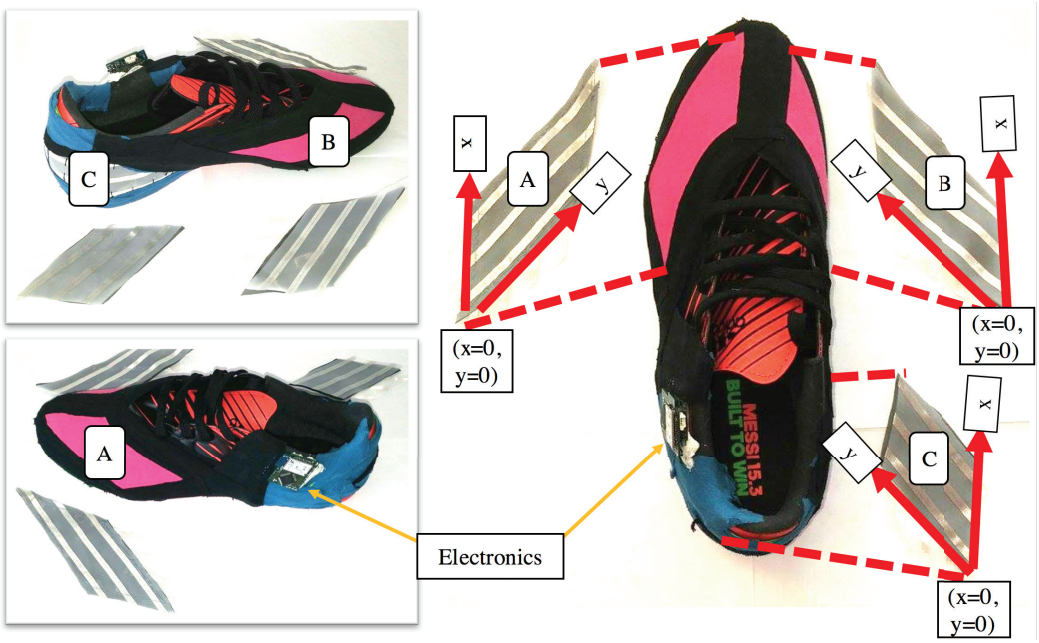

Figure 1. Instrumented shoe with dummy sensor patches on the side

- We developed different methods to extract information relevant for shot analysis from the pressure mapping data. Specifically we consider shots with different foot rotation around the leg axle, different speeds, and shift the impact center on the ball to the left and right.
- We evaluated our systems under controlled conditions. To this end we used a "kicking robot leg" (see Figure 9) which is the standard method used by the shoe manufacturer to systematically and quantitatively evaluate new soccer shoes and balls. We varied the angle from $-20°$ to $50°$, and the leg swing speed from amateur level ($10m/s$) to professional level ($20m/s$), overall 15 combinations plus two additional conditions for off-center impact.
- The best performance reaches near 100% accuracy and F-score for the 15 classes. With the same algorithms, the system isolates the off center variations from the before-mentioned 15 classes with 100% accuracy.

While we define the tests classes by the robot leg's parametric configurations (Table 1), the influence of those parameters on the actual flight path is well studied in the relevant literature [7] [19] and the development of the robot leg. In fact, under controlled conditions they may be directly used to predict ball trajectory. In a real game other factors may also play a role, however, from the point of view of the player; being able to control those parameters is a key aspect of being able to perform specific shots.

State of the Art

IMU based wearable systems

Akins [2] has extensively validated IMU sensors and magnetic field angular rate and gravity sensors embedded into soccer shoes and shin guards; compared with high speed cameras and vision markers; the data have shown a consistent correlation under all the testing activities. In the work of Schuldhaus, et al., [20] data from IMU-instrumented soccer shoes and shin guards are also proven to be able to detect several soccer related actions. Cappa, et al. compared in-shoe IMUs with wearable electromyography on the leg muscles to evaluate kinematics and muscle activation [5].

Pressure sensor based systems

Several insole foot planar pressure mapping systems can be found in other studies [1][10]. They are mainly used for gait analysis during walking, running, jumping, etc. ; however, the placement would not contribute to kicking a football. A 4-by-4 pressure mapping sensor [22] is installed over the shoe laces to visualize the kicking force and center of pressure. Yet the framework-focused pilot research has not included sufficient data in terms of shot variations, and the coverage of the shoe surface is limited on the shoe lace area.

HARDWARE

Instead of introducing add-ons to the shoe, our vision is that the sensing element should be eventually integrated inside the shoe surface material in an unobtrusive fashion that can be manufactured together with the shoes; to this end we have been close working with the shoe manufacturer. We use textile resistive pressure mapping sensing as in our previous work[24], and instrumented an adidas Messi 15.3 indoor soccer shoe. The sensors consist of two layers of fabric which have parallel metallic stripes, and one layer of pressure sensitive resistor fabric in the middle. The metallic stripes have 1.5cm pitch, and 0.7cm width. The sensors are separately tailored into 3 patches; instead of $90°$ crossings used in previous work, each of them have a $40°$ angle to accompany the profile of the shoe surface, indexed as A (outside front), B (inside front) and C (inside heel) as in Figure 1. Every crossing of the metallic stripes form a sensitive node (pixel), and the resolutions of A,

B, C are $3-by-4$, $3-by-4$ and $3-by-3$. We covered the front two patches with very thin and soft protective textile sport tapes, which do not significantly influence the sensors' readouts.

We scan the sensors with a micro-controller which has an 12-bit multi-channel analog-digital converter. The data is sent via Bluetooth to Android-powered devices (in our experiment we tested with a Samsung Galaxy Tab 2 or S6) at around 30KB/s datarate, reaching the scanning speed of $> 550Hz$ per sensing node. The smartphone/tablet saves the data for further processing. The sensors measure the pressure on the shoe surface cover material, which can be caused by higher speed ball impacts or the lower speed movements from the wearer's foot (i.e. toes). As shown in Figure 2, every $1.8ms$ there is a data point, and for every actual ball impact we have around ten observations, with the Bluetooth data bandwidth being the limitation.

While implementing the system, we keep in mind how plausible it is to eventually use it in real sports. With a small 800mAh Li-Po battery, the system can operate continuously for 8 hours. In the experiment of this work, we have only one side of the shoe paired to one Android device, we also implemented connecting two shoes (a pair) with one Android device, which has a slight drop of scanning speed from $550Hz$ to $420Hz$ per sensing node. The dimensions of the printed circuit board and the battery are $2.6 \times 3.5cm$ and $4.4cm \times 3.4cm$.

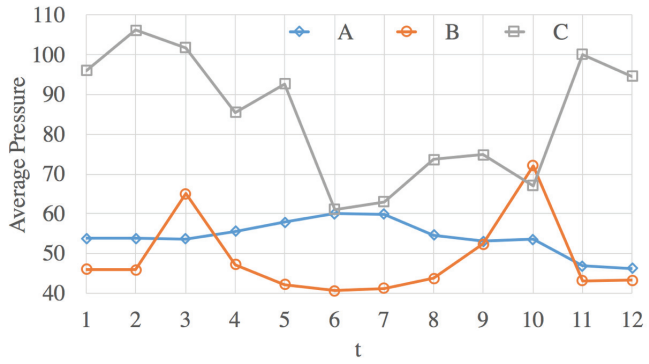

Figure 2. Average pressure from every sensor patch during a ball impact

ALGORITHMS

Preprocessing

The sensors provide a stream of data organized into 3 matrices $\{A,B,C\}$, each corresponding to one of the sensor patches: front-outside, front-inside and front-heel. The temporal resolution is approximately $1.8ms$. As shown in Figure 3, for each patch, this essentially gives us the impact pressure profile. In processing the data, we first apply a high-pass filter to the temporal data per pixel with passband of $2Hz$ to remove any static offset and drifting. We then resize the matrices by a factor of four in x and y dimensions. Then, we calculate the mean $w_{\{A,B,C\}}(t)$, centroid $(x,y)_{\{A,B,C\}}(t)$ and maximum $max_{\{A,B,C\}}(t)$ for each submatrix, denoting them as $S(t)$. We then segment the continuous temporal data stream based on

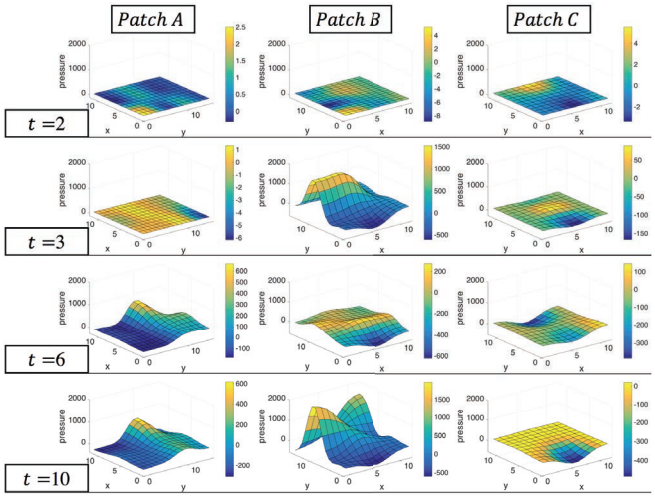

Figure 3. Example of pressure mapping readings during a ball impact, t corresponds to the data point in Figure 2; *Pressure* axis has a static range across all subplots while colormaps are adapted to individual matrix values

the highest peak value of mean $w_{\{A,B,C\}}(t)$ to detect individual ball contacts. Every segment i is a $90ms$ window centered at the peak. We refer to the the time span as time domain T_i. $S(t)$ of every data sample is a time-varying sequence $S_i(t), t \in T_i$.

Figure 4 shows that for an impact of the same class, $S(t)$ have reproducible patterns. (The class definition is explained later in **Evaluation**) Therefore, for every $t \in T_i$ we calculate the average of $S(t)$ from all training data samples. We use the result as a template $S_{Template}(t), t \in T_i$ for every specific class.

Feature Extraction

To extract features that best represent the force mapping signature of different types of impact, we have investigated multiple methods.

Method 1: Template Matching

For every iteration of the cross validation, the templates $S_{Template}(t), t \in T_i$ are calculated anew from the training samples, excluding testing samples, and every class has one set of templates. We then calculate the mean of multiplication, and mean of subtraction between the template and every data sample i, using the products as features $F_1(i)$. Since every $S_{Template}(t), t \in T_i$ has 12 members, and overall 15 classes, $F_1(i)$ has 180 members.

Method 2: Wavelet Analysis

In Method 1, when there is a new training sample, the templates are recalculated and all the features will change accordingly. For a more generic algorithm, we use wavelet analysis with the LTFAT toolbox [17]. First we use Mallat's fast wavelet transform (fwt) algorithm [13] on every $S_i(t), t \in T_i$ with 10 iterations of the Daubechies-8 wavelet [8]. It produces a scaleogram of fwt coefficients of 11 sub-bands as shown in Figure 6. For every sub-band, we calculate the mean of coefficients; for sub-bands $d9-d1$, we also calculate the variance, standard deviation, skewness and kurtosis that describes the distribution of the wavelet coefficients. For every data sample, $47 \times 12 = 564$ features are used as $F_2(i)$.

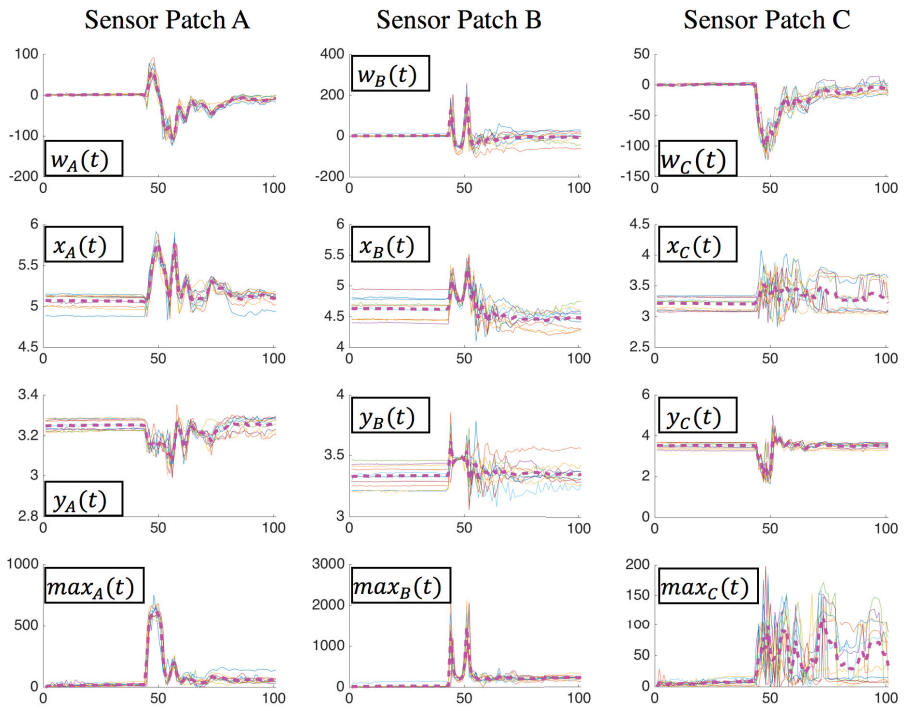

Figure 4. Data samples of class $\alpha = 40°, \upsilon = 10$, thin solid lines are raw data $S_i(t)$, and thick dash lines are template $S_{Template}(t)$

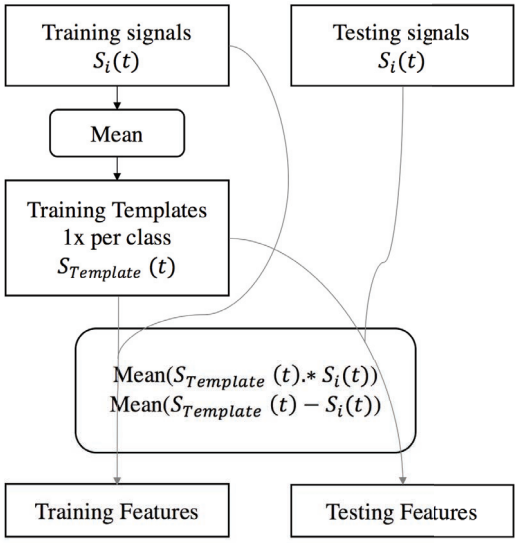

Figure 5. Method 1 algorithm

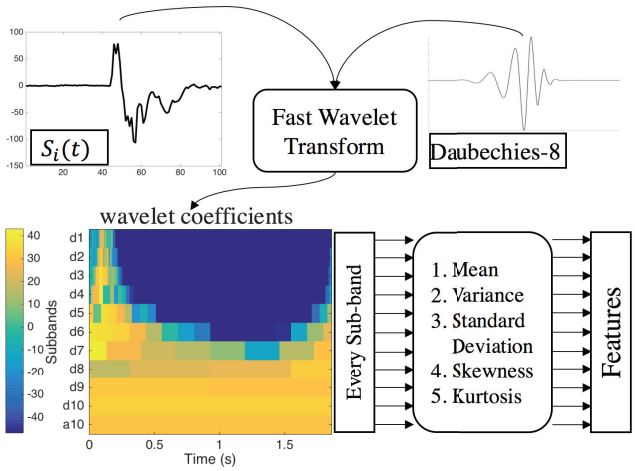

Figure 6. Method 2 algorithm

Method 3: 2-Dimensional Analysis

While in Method 1 and 2, $(x,y)_{\{A,B,C\}}(t)$ and $max_{\{A,B,C\}}(t)$ are beneficial from the pressure mapping matrix in contrast against single-sensor FSR installments, the entire 2-dimensional mapping information is not fully used. For every data sample, we take the stream of 2D pressure mapping $PM_{(i,\{A,B,C\})}$, for every pixel, we apply zero-phase high-pass filtering to remove DC. Then four special pressure mapping frames are extracted: we isolate the positive and negative values per pixel and calculate the mean per pixel as $PM+_{(i,\{A,B,C\})}$ and $PM-_{(i,\{A,B,C\})}$, the mean value of every pixel as $PMmean_{(i,\{A,B,C\})}$ ($PMmean_{(i,\{A,B,C\})}$ is similar to the long exposure method in photography), and the frame at the time when the sum of $PM_{(i,\{A,B,C\})}(t)$ is maximum within the data sample, as $PMmax_{(i,\{A,B,C\})}$. We then calculate ten image moments of those speical frames (first three central moments and Hu's seven moments) [12]. Image moments are image descriptors that can represent certain properties of the pixel density distribution. Overall, 120 image moments are extracted for every data sample as features $F_3(i)$.

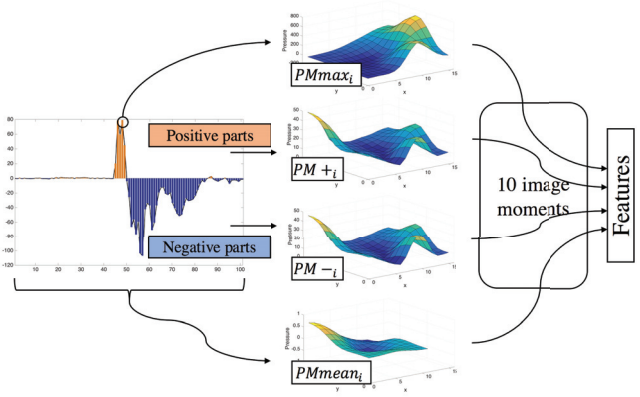

Figure 7. Method 3 algorithm

EVALUATION

Robotic Leg

To test the sensors' capability of measuring different football shot angles and forces, we conducted an experiment with a robotic leg that is designed specifically for simulating football kicking actions as shown in Figure 9. Its mechanical details and the variation of ball flight paths are documented [23]. The robotic leg has a controlled motor at the thigh joint, which offers a controllable leg swing speed υ. At the ankle joint, there are two adjustable hinges:

- the angle of the foot's rotation around the length axle of the leg cylinder α;
- the angle of the foot's tilt around the radius direction of the leg cylinder β.

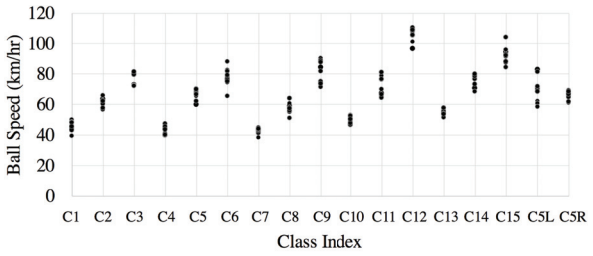

Figure 8. measured ball speed distribution

Experiment Design

During the experiment, we use adidas Brazuca 2014 match balls with 0.6 Bar pressure. The foot-ball impact position is marked on the ball with a laser cross and is controlled to be at the vertical center of the ball from the view of the foot as in Figure 13. We define different classes of kicking with various α and υ combinations listed in Table 1. Since in some of the combinations, the ball would fire to the lab ceiling or out of the protected field at the speed of $100km/hr$, we adjust the β angle, horizontal impact position of the ball and the orientation of the robotic leg's platform to ensure that the trajectory will point towards the goal direction like a realistic shot. With real players, the trajectory is typically controlled by the combination of multiple factors such as the foot angle and the body orientation of the players.

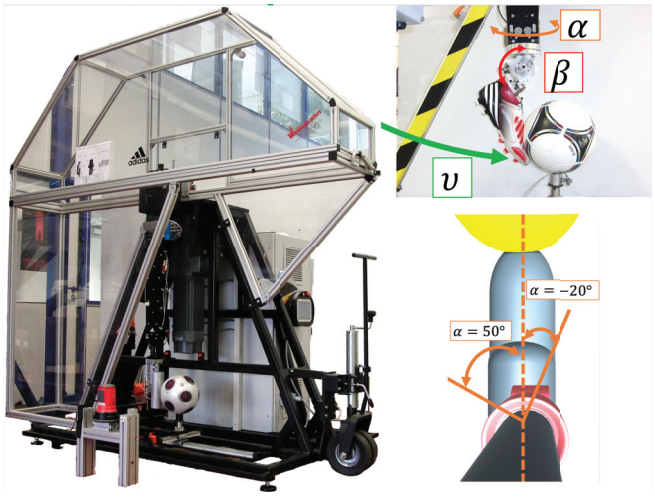

Figure 9. Graphical illustration of the kicking robot leg, ankle angles α, β and leg speed *upsilon*. Free view (left), side view (up-right) and top view (down-right)

Table 1. Class Definition

	$\upsilon = 10$	$\upsilon = 15$	$\upsilon = 20$
$\alpha = 50°$	C1	C2	C3
$\alpha = 40°$	C4	C5	C6
$\alpha = 20°$	C7	C8	C9
$\alpha = 0°$	C10	C11	C12
$\alpha = -20°$	C13	C14	C15

The speed of the ball is measured with a combination of hawk-eye system and speed radar. The ball speed ranges from around $40km/hr$ at $\upsilon = 10m/s$ to over $100km/hr$ at $\upsilon = 20m/s$, and varies with different impact insertion angle from the foot to the ball.

With multiple footballs, we fire the ball 10 times per class, overall 170 shots are recorded. Before every shot, the shoe is manually readjusted on the robot's foot to introduce some variance of the initial position. The ball speeds are shown in Figure 8; to compare the variance and offer a reference for further classification accuracy, the average $StandardDeviation/MeanValue$ ratio of ball speeds is 5.74%.

Visualizing

Combining $(x,y)_{\{A,B,C\}}(t)$, and $max_{\{A,B,C\}}(t)$, the track of the center of impact with its intensity can be visualized as in Figure 10, where the position of circles are $(x,y)_{\{A,B,C\}}(t)$ coordinates and the radius of circles are scaled to $max_{\{A,B,C\}}(t)$. The method is similar to the work by Weizman, et al. [22]. From it, it can be concluded that as the swing speed increases, the impact has greater intensity over its curve; and different α angles result in distinct tracks of impact center. It is also very obvious while the shoe rotates from $\alpha = 50°$ to $\alpha = -20°$ as in Figure 9, the major impact area shifts from the heel part to more on the front-inner, then front-outside.

Cross-validation

To evaluate if it is possible to distinguish the α angle and leg speed combinations defined during the experiment from the sensor data, we carry out cross-validation with standard

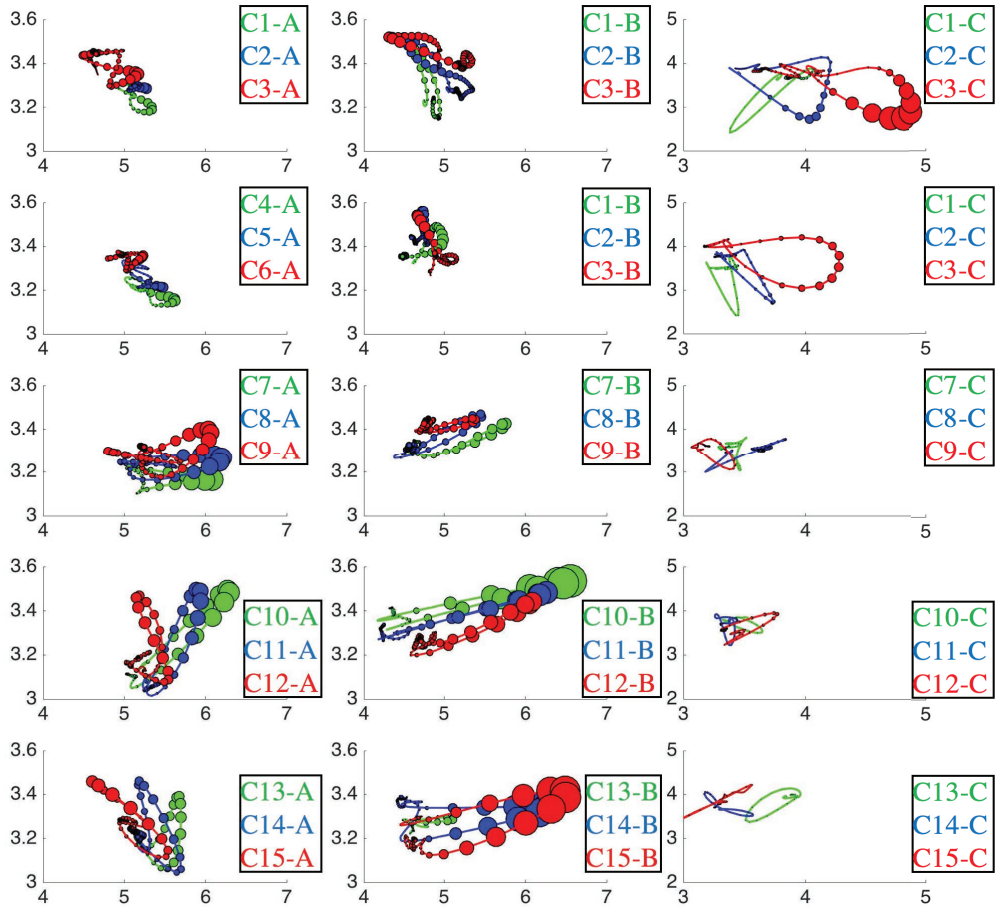

Figure 10. Combined visualization of impact center $((x,y)_{\{A,B,C\}}(t)$ (on horizontal and vertical axes) and $max_{\{A,B,C\}}(t))$ (circle radius) of all classes from $\{C1-C15\}$. Circles' radii are scaled to the same factor.

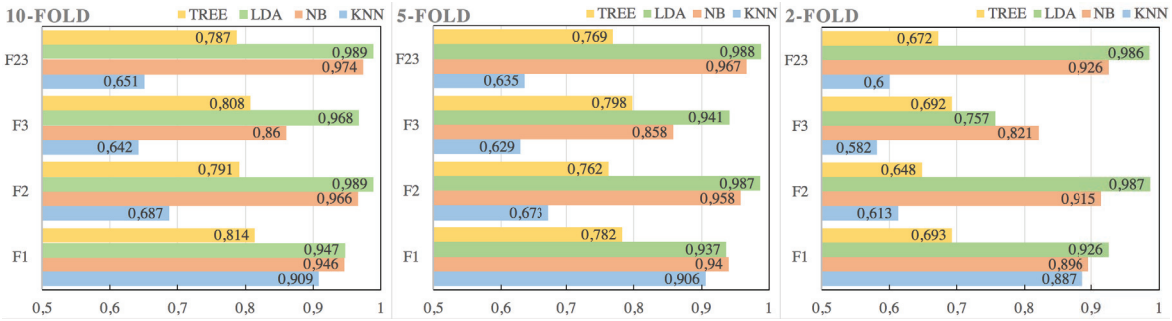

Figure 11. F-scores of cross-validation on different feature sets $F_1(i)$, $F_2(i)$,$F_3(i)$ and $F_{23}(i)$

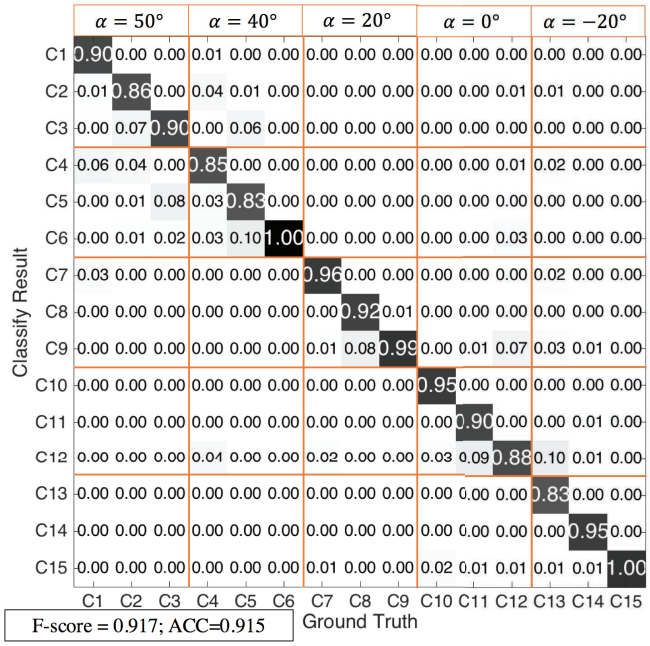

Figure 12. Example confusion matrix of $F_2(i)-NB-2-Fold$ with 0.915 F-score

classifiers: KNN, Naive Bayes, linear discriminant analysis and decision tree to compare the performances. We perform 10-fold, 5-fold and 2-fold cross-validation, to examine the influence of less training data. For every feature-classifier-fold combination we run the algorithm for 20 iterations and calculate the F-scores $(2\times(Precision\times Recall)/(Precision+Recall))$ from the average value of confusion matrices from the 20 iterations.

The resulting F-scores are summarized in Figure 11. In 10-fold, for $F_1(i)$ feature set, multiple classifiers (KNN, NB, LDA) generate similar classification result; with $F_2(i)$, $F_3(i)$, LDA has higher F-score, but the other classifiers have poorer result; on average, combined $F_{23}(i)$ has slightly better result than individual $F_2(i)$, $F_3(i)$. As the fold number decreases, there are less training data samples and more testing, and most of the classifiers' f-scores decrease; however, with $F_2(i)$ from wavelet analysis, LDA classifier, the f-score is robust against such condition.

To show where the actual miss-classifications are located, we take the confusion matrix from $F_2(i)-NB-2-Fold$ with 0.915 F-score as an example in Figure 12. It can be seen that most confusions happen between same α angle with different leg speeds, as well as between adjacent α angles. This shows that even if the data sample is classified as a different type, the actual foot angle and swing speed lies within the adjacent possibilities.

Shift of Kicking Center

As explained in Section **Experiment Design**, the impact position on the ball is regulated to be at the vertical center with a laser. To evaluate whether the sensor is capable to distinguish the change of the kicking center, we move the ball center $30mm$ away from the vertical center to both the left and right, at the combination of $\alpha=40^\circ$ and $\upsilon=15m/s$, giving them the class index of *C5L* and *C5R* as shown in Figure 13. This is primarily to introduce spinning variance on the ball.

With feature set $F_2(i)$ derived by wavelet analysis, and linear discriminant analysis classifier, we reach accuracy and F-score of both 100%. Yet it is possible that moving the center of the ball might fall into the impact condition of other α angles, we therefore combine $\{C5L,C5R\}$ with $\{C1-C15\}$, overall 17 classes. In a 10-fold cross-validation with $F_2(i)$ features and LDA classifier, as shown in Figure 14, the change of the ball impact center is distinctly different from other classes by the information from our sensor.

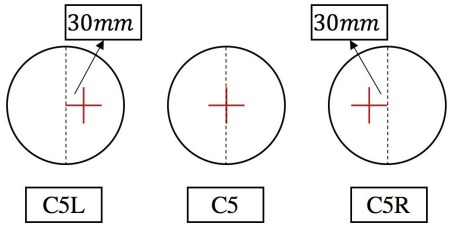

Figure 13. Illustration of the impact center on the ball with the view from the foot, and defination of Class $\{C5L,C5,C5R\}$ ($\alpha=40^\circ$ and $\upsilon=15m/s$)

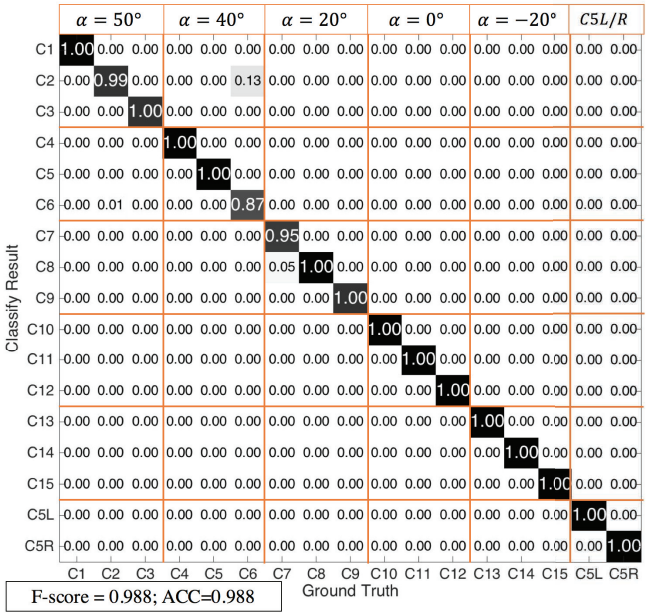

Figure 14. Confusion matrix with F_2 feature set and LDA classifier, 10-fold of 17 classes including Class $\{C5L,C5R\}$

CONCLUSION AND OUTLOOK

The results presented in this paper show that a simple textile pressure matrix sensor embedded in a soccer shoe can provide sufficient information to reliably distinguish different ways in which the players foot strikes the ball. The evaluation was done in the same was as the shoe and ball manufacturer evaluates the performance of shoes and balls, which is through a robotic leg that provides well defined, reproducible shots.

Having established that we can accurately capture the parameters of the foot ball interaction, the next step would be to combine this functionality with inertial sensors in the shoe and investigate how well the characteristics of the shot can be predicted in a real game.

The sensor design has been done together with the shoe manufacturer and in the next version, the sensors will be integrated under the standard upperlayer material of the shoe, making it indistinguishable from standard shoe. The electronics can be integrated in the sole as has been already demonstrated by the shoe manufacturer for inertial sensors.

ACKNOWLEDGMENTS

We thank our colleagues from adidas AG who supported the data acquisition and provided expertise that greatly assisted the research. This work was further supported by the Bavarian Ministry of Economic Affairs and Media, Energy and Technology and by the EU FET Open Project SimpleSkin

REFERENCES

1. Abdul Hadi Abdul Razak, Aladin Zayegh, Rezaul K Begg, and Yufridin Wahab. 2012. Foot plantar pressure measurement system: A review. *Sensors* 12, 7 (2012), 9884–9912.
2. Jonathan Stephen Akins. 2013. *Development and evaluation of instrumented soccer equipment to collect ankle joint kinematics in the field*. Ph.D. Dissertation. University of Pittsburgh.
3. Sarah Barber, Stephen J Haake, and Matt Carré. 2006. Using CFD to understand the effects of seam geometry on soccer ball aerodynamics. In *The Engineering of Sport 6*. Springer, 127–132.
4. Ken Bray and David Kerwin. 2003. Modelling the flight of a soccer ball in a direct free kick. *Journal of sports sciences* 21, 2 (2003), 75–85.
5. Paolo Cappa, Alessandra Pacilli, Eduardo Palermo, and Stefano Rossi. 2015. Mobile motion capturing in sport session based on Inertial Measurement Units. (2015).
6. Jingyuan Cheng, Mathias Sundholm, Bo Zhou, Marco Hirsch, and Paul Lukowicz. 2016. Smart-surface: Large scale textile pressure sensors arrays for activity recognition. *Pervasive and Mobile Computing* (2016).
7. Je Youn Choi, Byung Rok So, Byung-Ju Yi, Wheekuk Kim, and Il Hong Suh. 2005. Impact based trajectory planning of a soccer ball in a kicking robot. In *Robotics and Automation, 2005. ICRA 2005. Proceedings of the 2005 IEEE International Conference on*. IEEE, 2834–2840.
8. Ingrid Daubechies. 1992. Ten Lectures on Wavelets. (1992).
9. Neville De Mestre. 1990. *The mathematics of projectiles in sport*. Number 6. Cambridge University Press.
10. Eric Eils, Markus Streyl, Stefan Linnenbecker, Lothar Thorwesten, Klaus Völker, and Dieter Rosenbaum. 2004. Characteristic plantar pressure distribution patterns during soccer-specific movements. *The American Journal of Sports Medicine* 32, 1 (2004), 140–145.
11. Sungchan Hong and Takeshi Asai. 2014. Effect of panel shape of soccer ball on its flight characteristics. *Scientific reports* 4 (2014).
12. Ming-Kuei Hu. 1962. Visual pattern recognition by moment invariants. *Information Theory* 8, 2 (February 1962), 179–187.
13. S. Mallat. 1998. A wavelet tour of signal processing. (1998).
14. Rabindra D Mehta and Jani M Pallis. 2001. Sports ball aerodynamics: effects of velocity, spin and surface roughness. *Minerals, Metals and Materials Society/AIME, Materials and Science in Sports(USA),* (2001), 185–197.
15. Luca Oggiano and Lars Sætran. 2010. Aerodynamics of modern soccer balls. *Procedia Engineering* 2, 2 (2010), 2473–2479.
16. Ignacio Palacios-Huerta. 2004. Structural changes during a century of the worldâĂŹs most popular sport. *Statistical Methods and Applications* 13, 2 (2004), 241–258.
17. Zdeněk Průša, Peter L. Søndergaard, Nicki Holighaus, Christoph Wiesmeyr, and Peter Balazs. 2014. The Large Time-Frequency Analysis Toolbox 2.0. In *Sound, Music, and Motion*. Springer International Publishing, 419–442. DOI:http://dx.doi.org/{10.1007/978-3-319-12976-1_25}
18. Thomas Reilly and David Gilbourne. 2003. Science and football: a review of applied research in the football codes. *Journal of Sports Sciences* (2003).
19. Hagen Schempf, Charles Kraeuter, and Mike Blackwell. 1995. ROBOLEG: A robotic soccer-ball kicking leg. In *Robotics and Automation, 1995. Proceedings., 1995 IEEE International Conference on*, Vol. 2. IEEE, 1314–1318.
20. Dominik Schuldhaus, Constantin Zwick, Harald Koerger, Eva Dorschky, Robert Kirk, and Björn Eskofier. 2015. Inertial Sensor-Based Approach for Shot/Pass Classification During a Soccer Match. In *KDD Workshop on Large-Scale Sports Analytics 2015*, SIGKDD (Ed.). 1–4.
21. Mathias Sundholm, Jingyuan Cheng, Bo Zhou, Akash Sethi, and Paul Lukowicz. 2014. Smart-mat: Recognizing and counting gym exercises with low-cost resistive pressure sensing matrix. In *Proceedings of the 2014 ACM international joint conference on pervasive and ubiquitous computing*. ACM, 373–382.
22. Yehuda Weizman and Franz Konstantin Fuss. 2015. Sensor Array Design and Development of Smart Sensing System for Kick Force Visualization in Soccer. *Procedia Technology* 20 (2015), 138–143.
23. Kerstin Witte and Harald Körger. 2010. Optimierung der Ballschussmaschine Robyleg II und Untersuchung des Deformationsverhaltens von Fußbäallen. (2010).
24. Bo Zhou, Mathias Sundholm, Cheng Jingyuan, Heber Cruz, and Paul Lukowicz. 2016. Never Skip Leg Day: A Novel Wearable Approach to Monitoring Gym Leg Exercises. (2016).